Photoinduced Multistep Electron Transfer in an Oligoaniline−Oligo(*p*-phenylene Vinylene)−Perylene Diimide Molecular Array

Alicia Marcos Ramos, Edwin H. A. Beckers, Ton Offermans, Stefan C. J. Meskers, and René A. J. Janssen*

Molecular Materials and Nanosystems, Laboratory of Macromolecular and Organic Chemistry, Eindhoven University of Technology, Post Office Box 513, 5600 MB Eindhoven, The Netherlands, and Dutch Polymer Institute, Post Office Box 902, 5600 AX Eindhoven, The Netherlands

Received: March 8, 2004; In Final Form: July 13, 2004

Photoinduced multistep electron transfer has been studied in two symmetrical oligoaniline−oligo(*p*-phenylene vinylene)−perylene diimide−oligo(*p*-phenylene vinylene)−oligoaniline (OAn−OPV−PERY−OPV−OAn) multichromophore arrays with fluorescence and transient absorption spectroscopy in the femtosecond and nanosecond time domains. The arrays consist of a symmetrical donor(2)−donor(1)−acceptor−donor(1)−donor(2) arrangement, with two OAn−OPV segments coupled to a central PERY unit via a direct linkage (**1**) or a saturated spacer (**2**). Photoexcitation gives the OAn−OPV$^{+\bullet}$−PERY$^{-\bullet}$−OPV−OAn as the primary charge-separated state. For **1** the transfer is extremely fast ($k_{CS} > 1000$ ns^{-1}) in polar and apolar solvents, while the rate constants for recombination differ and are significantly higher in polar solvents than in apolar solvents because recombination occurs in the Marcus inverted region. Charge separation and charge recombination are slower in **2**, because the saturated spacer reduces the electronic coupling between OPV donor and PERY acceptor. The primary OAn−OPV$^{+\bullet}$−PERY$^{-\bullet}$−OPV−OAn charge-separated state can rearrange in a charge-shift reaction to the OAn$^{+\bullet}$−OPV−PERY$^{-\bullet}$−OPV−OAn state. This charge shift is exergonic and competes with fast charge recombination. In polar solvents the efficiency of the charge shift is about 0.22 and 0.28 for **1** and **2**, respectively, and only weakly dependent on the polarity. In toluene the two charge-separated states are nearly isoenergetic for **1,** and hence, no shift is observed in toluene. The OAn$^{+\bullet}$−OPV−PERY$^{-\bullet}$−OPV−OAn charge-separated state has a long lifetime as a result of the negligible interaction between the distant OAn$^{+\bullet}$ and PERY$^{-\bullet}$ redox sites and can be observed up to several microseconds.

Introduction

Inspired by intriguing future application in molecular electronics, photocatalysis, and artificial photosynthesis, photoinduced energy and electron transfer in covalently linked donor−acceptor molecules attract considerable attention.[1] For practical applications, it is often of interest to combine a high rate for charge separation with a low rate for charge recombination. For this purpose multichromophoric arrays have been designed in which the initial photoinduced charge separation is followed by charge migration reactions along a well-defined redox gradient that ultimately provides the spatial separation of the photogenerated charges that is essential to lower the rate for charge recombination. Various elegantly designed triads, tetrads, etc., have been synthesized and investigated in detail.[2,3]

Multistep electron transfer, or charge migration, is possibly also the origin of the longevity of charges in solid-state blends of donor and acceptor materials used in organic and polymer solar cells.[4] In these devices, excitons, created by the absorption of light, dissociate at the donor−acceptor interface, forming an electron−hole pair. When this electron and hole escape from geminate recombination and diffuse away from the interface,[5] they can be collected at electrodes as a photocurrent.

Recent studies on covalently linked oligo(*p*-phenylene vinylene) (OPV) donors and perylene diimide (PERY) acceptors in liquid crystalline OPV−PERY−OPV triads,[6,7] π-stacks of hydrogen-bonded OPV−PERY−OPV trimers,[8] and alternating (OPV−PERY)$_n$ copolymers[9] have revealed that photoinduced electron transfer can be extremely fast in solution (<1 ps) but that the lifetime of the charge-separated state is generally rather short (<1 ns). Because of their high absorption coefficients in the visible region and their charge transport properties, OPV[10−15] and PERY[16−20] chromophores have also attracted interest for organic solar cells.

With the aim to extend the lifetime of the charge-separated state, two new multichromophoric molecular arrays incorporating a central OPV−PERY−OPV triad augmented with two *p*-oligoaniline (OAn) moieties as additional donors have been designed (**1** and **2**, Figure 1). We will show that in both donor-(2)−donor(1)−acceptor−donor(1)−donor(2) arrays the OAn and OPV donors and PERY acceptors are essentially electronically decoupled from each other in the ground state and operate essentially as isolated redox-active segments.[21] The two arrays differ in the connectivity between the central PERY segment and the OPV donors. In **1**, the OPV and PERY units are directly connected, providing a close proximity. Because the OPV and PERY chromophores are likely not coplanar in **1** and there is a nodal plane at the nitrogen diimide in the frontier orbitals, there is no direct conjugation in **1**, even though all atoms are sp^2-hybridized. In **2**, the OPV−PERY distances are longer and the conjugation is fully interrupted by saturated bonds. The redox potentials of the OAn, OPV, and PERY segments favor the

* Corresponding author: Phone (+)31-40-2473597; fax (+)31-40-2451036; e-mail r.a.j.janssen@tue.nl.

10.1021/jp048971e CCC: $27.50
Published on Web 09/10/2004

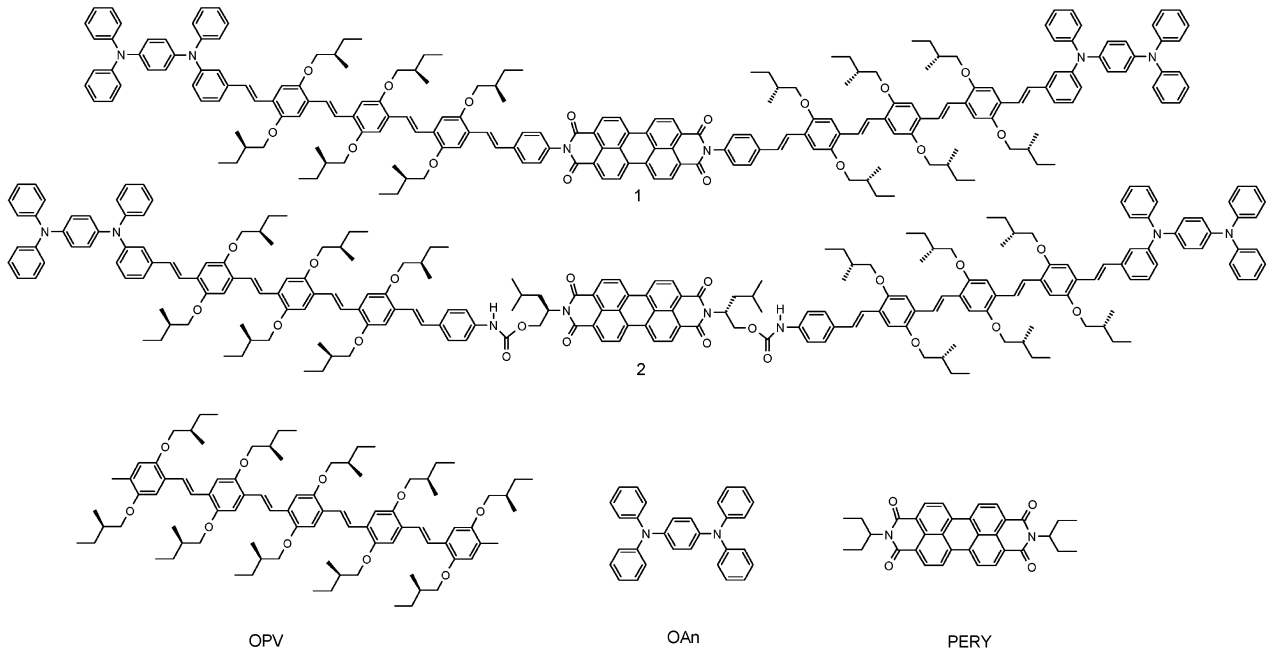

Figure 1. Chemical structures of arrays **1** and **2** and reference compounds OPV, OAn, and PERY.

$OAn^{+\bullet}-OPV-PERY^{-\bullet}-OPV-OAn$ state as the lowest-energy charge-separated state after photoexcitation. Arrays **1** and **2** have been studied by photoluminescence and transient absorption spectroscopy in solvents of different polarity to investigate the photoinduced multistep electron transfer. The kinetics of charge separation, migration, and recombination have been determined and are rationalized in terms of Marcus theory, by use of a continuum model to describe the Gibbs energy.

Results

Synthesis. For synthesizing **1** (Scheme 1), aldehyde **3**[22] was coupled to diethyl 4-nitrobenzyl phosphonate **4** via a Wittig−Horner reaction, affording nitro compound **5**. Subsequent reduction of the nitro group to the terminal amine **6** was achieved by use of stannous dichloride and ethanol in ethyl acetate. Condensation of **6** with 3,4:9,10-perylenetetracarboxylic dianhydride in imidazole with catalytic amounts of $Zn(OAc)_2$ afforded **1**. Pure **1** was obtained via extensive column chromatography and preparative size-exclusion chromatography, which resulted in a low yield for this last step. For the synthesis of array **2** (Scheme 1), the amine function in OAn−OPV **6** was reacted with phosgene in toluene to yield isocyanate **7**. Dihydroxy-terminated perylene diimide **8** was obtained via a 2-fold condensation of (*S*)-(+)-leucinol with 3,4:9,10-perylenetetracarboxylic dianhydride. Array **2** was then prepared by 2-fold reaction of isocyanate **7** with the hydroxyl functions of **8**, with dibutyltin dilaurate as a catalyst. All compounds were characterized by ^1H NMR spectroscopy, mass spectrometry, and size-exclusion chromatography.

Absorption Spectroscopy. The UV−visible absorption spectrum of **1** in toluene (Figure 2a) exhibits two strong absorption bands, one centered at 327 nm and the other featuring vibronic fine structure with peaks at 464, 494, and 532 nm. For direct comparison, the absorption spectra of the OAn, OPV, and PERY reference compounds (Figure 1) are also plotted in Figure 2a. All chromophores contribute to the absorption of the UV region of **1**, but the absorption in the visible region is dominated by the $\pi-\pi^*$ transitions of the OPV and PERY chromophores. The characteristic vibronic fine structure of the PERY chromophore is clearly present in the visible region.

SCHEME 1: Synthesis of OAn−OPV−PERY−OPV−OAn 1 and 2[a]

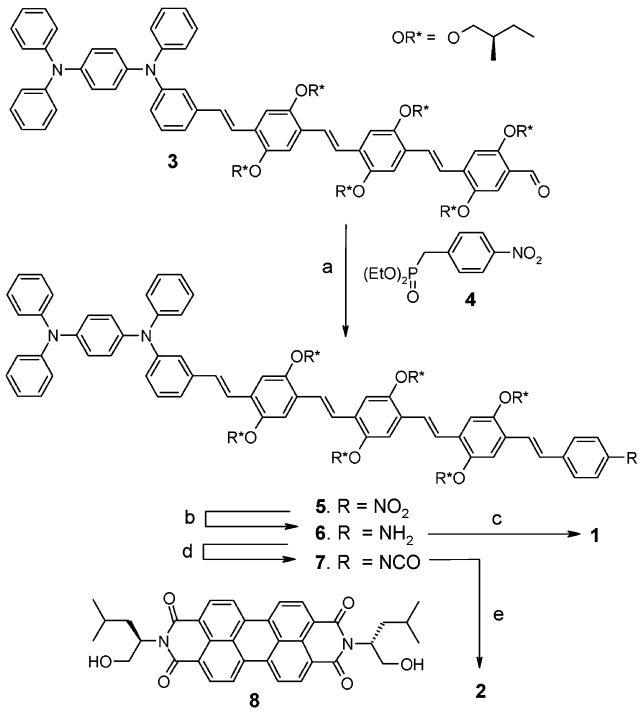

[a] (a) *t*-BuOK, DMF/THF (2:1), rt, 2 h, 86%. (b) $SnCl_2 \cdot H_2O$, EtOH, EtOAc, 95 °C, 5 h, 70%. (c) 3,4:9,10-Perylenetetracarboxylic dianhydride, imidazole, $Zn(OAc)_2$, 160 °C, 4 h, 9%. (d) Phosgene, toluene, 95 °C, 16 h, 100%. (e) Dibutylin dilaurate, CH_2Cl_2, reflux, 20 h, 47%.

The UV−visible absorption spectrum of **2** (Figure 2b) recorded in tetrahydrofuran (THF) also consists of the overlapping absorptions of the OAn, OPV, and PERY chromophores. The low-energy absorption band at 532 nm of the PERY chromophore exhibits a lower intensity for **2** than for **1**. In *o*-dichlorobenzene, the spectrum is slightly shifted to higher wavelengths but otherwise is rather similar. In toluene (Figure 2b), the absorption spectrum of **2** shows a reduced intensity of the peak at 532 nm and a weak contribution above 550 nm,

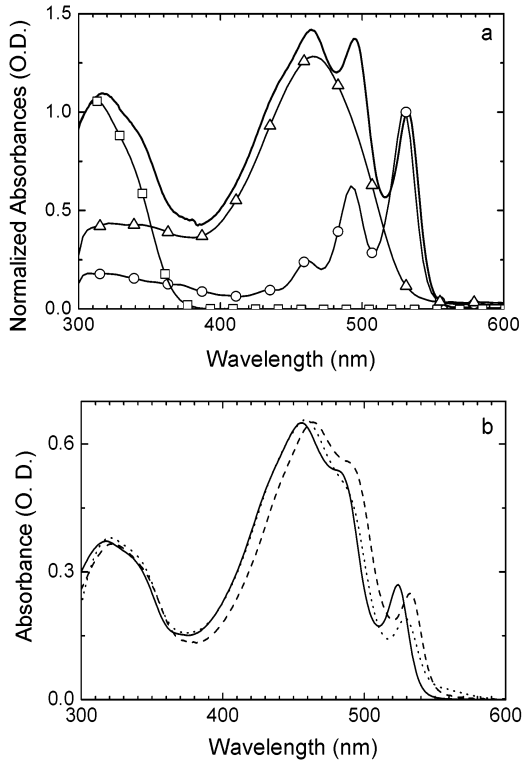

Figure 2. (a) UV−visible absorption spectra of the OAn−OPV−PERY−OPV−OAn array **1** (—) and model compounds OAn (□), OPV (△), and PERY (○) recorded in toluene solution, normalized to the same molar concentration. (b) UV−visible absorption spectra of the OAn−OPV−PERY−OPV−OAn array **2** in tetrahydrofuran (—), ODCB (− − −), and toluene (···).

which may indicate some aggregation as a consequence of intermolecular hydrogen bonding and $\pi-\pi$ interactions.[7] A similar reduction of intensity of the lowest-energy PERY absorption has also been observed in a macrocyclic compound in which OPV and PERY chromophores were positioned on top of each other,[9] and more recently in main-chain OPV polymers with back-folded pendant PERY chromophores.[23] In these examples the reduction could be explained by an electronic interaction between the two chromophores. When these are in close proximity and the angle between their transition dipole moments is less than the magic angle of 54.7°, exciton coupling will increase the probability for the high-energy transition of the OPV segments compared to that of the low-energy transition of the perylene diimide, resulting in decreased absorption at longer wavelengths. Because of the flexible linker between OPV and PERY, the required back-folding for this electronic coupling is possible in **2**.

Electrochemistry. The electrochemical properties of **1** and **2** and of the reference compounds OAn, OPV, and PERY were investigated by cyclic voltammetry in dichloromethane. The redox potentials are collected in Table 1. Reversible reduction of the PERY acceptor in **1** occurs at half-wave potentials of −0.53 and −0.76 V. Array **1** could be oxidized in four consecutive reversible oxidations at +0.53 and +1.03 V corresponding to the OAn segment and at +0.76 and +0.96 for the OPV moiety (Table 1). In dichloromethane, also four oxidation waves were observed for **2** at +0.53 and +1.07 V (OAn) and at +0.74 and +0.90 V (OPV). In this solvent no reduction was observed for **2**. We assume that the reduction of **2** in dichloromethane is hampered by aggregation. In accordance, the UV−visible spectrum of **2** in dichloromethane is similar to that in toluene and indicative of aggregation. In THF, however,

TABLE 1: One-Electron Half-Wave Redox Potentials ($E°$) of OAn, OPV, PERY, and OAn−OPV−PERY−OPV−OAn[a]

compound	$E°_{red}$ (V)	$E°_{ox}$ (V)
OAn		0.53/1.02
OPV		0.73/0.80
PERY	−0.65/−0.85	
array **1**	−0.53/−0.76	0.53/0.76/0.96/1.07
array **2**	−0.60/−0.89[b]	0.53/0.74/0.90/1.07

[a] Redox potentials are given vs SCE and calibrated with Fc/Fc^+ (in dichloromethane with 0.1 M $TBAPF_6$). [b] Measured in THF.

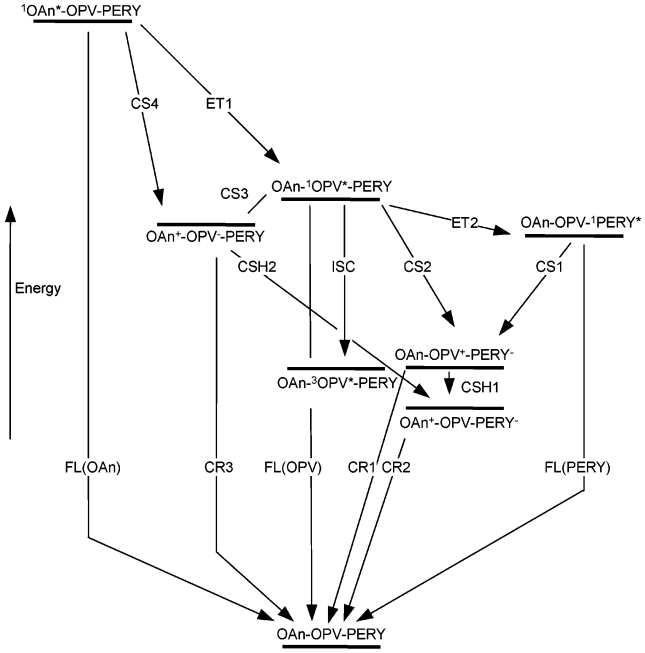

Figure 3. Schematic energy levels (in THF) and photoinduced processes in OAn−OPV−PERY−OPV−OAn arrays **1** and **2**. CS = charge separation, CR = charge recombination, ET = energy transfer, CSH = charge shift, FL = fluorescence, ISC = intersystem crossing.

where aggregation is not observed, the cyclic voltammogram of **2** exhibits the two reduction waves at −0.60 and −0.89 V corresponding to the PERY moiety.

Comparison with the model compounds OPV, OAn, and PERY (Figure 1) reveals that the first and second oxidation potentials of **1** and **2** are not strongly affected by linking the OPV and OAn chromophores (Table 1). In contrast, the reduction potential of the PERY acceptor depends on the nature of the imide functionality. The reduction potentials of **1** and **2** are shifted by +0.12 and +0.05 V, respectively, with respect to that of the PERY reference compound (−0.65 V). For **2** the shift is less, owing to the similar alkyl substitution as in the PERY reference.

Energetic Considerations. Figure 3 shows the photophysical processes that can occur in these arrays upon illumination. Photoexcitation initially generates the localized singlet-excited states with energies at 3.40, 2.39, and 2.33 eV for ^{1}OAn*, ^{1}OPV*, and ^{1}PERY*, respectively, depending on the excitation energy used. Each of these states can decay via the normal processes [fluorescence (FL), intersystem crossing (ISC), or thermal decay]. More interesting, however, is the interaction between the chromophores in the excited state. Energy transfer (ET) can occur along the line ^{1}OAn* → ^{1}OPV* → ^{1}PERY*. In addition, charge separation (CS) between adjacent chromophores would generate the $OAn-OPV^{+\bullet}-PERY^{-\bullet}-OPV-OAn$ or $OAn^{+\bullet}-OPV^{-\bullet}-PERY-OPV-OAn$ states. Subsequently, these charge-separated states can decay to the ground state via charge

TABLE 2: Rate Constants for Charge Separation and Recombination and Efficiency of Charge Shifts for Arrays 1 and 2 in Different Solvents

process	**1** in toluene	**1** in THF	**2** in THF
CS1/CS2	$>1000 \times 10^9\,s^{-1}$	$>1000 \times 10^9\,s^{-1}$	$285 \times 10^9\,s^{-1}$
CR1	$2.7 \times 10^9\,s^{-1}$	$83 \times 10^9\,s^{-1}$	$10 \times 10^9\,s^{-1}$
CR2		$<0.1 \times 10^9\,s^{-1}$	$<0.1 \times 10^9\,s^{-1}$
CSH1	0%	22%	28%

recombination (CR) or evolve to the more distant $OAn^{+\bullet}$–OPV–$PERY^{-\bullet}$–OPV–OAn state via a charge shift (CSH).

In contrast to the localized singlet-excited states, the energy of the charged separated states is strongly influenced by the polarity of the medium. Equation 1 provides a means of estimating the energies of the charged states as a function of the polarity of the solvent and distance between chromophores:[24]

$$\Delta G^\circ = e[E_{ox}(D) - E_{red}(A)] - E_{00} - \frac{e^2}{4\pi\epsilon_0\epsilon_s R_{cc}} - \frac{e^2}{8\pi\epsilon_0}\left(\frac{1}{r^+} + \frac{1}{r^-}\right)\left(\frac{1}{\epsilon_{ref}} - \frac{1}{\epsilon_s}\right) \quad (1)$$

In this equation, $E_{ox}(D)$ and $E_{red}(A)$ are the oxidation and reduction potentials of the donor and acceptor molecules or moieties measured in a solvent with relative permittivity ϵ_{ref} ($= 8.93$ for dichloromethane), E_{00} is the energy of the excited state from which the electron transfer occurs, and R_{cc} is the center-to-center distance of the positive and negative charges in the charge separated state. The radii of the positive and negative ions are given by r^+ and r^-, ϵ_s is the relative permittivity of the solvent, $-e$ is the elemental charge, and ϵ_0 is the vacuum permittivity.

The change in Gibbs energy for charge separation, charge shift, and charge recombination in **1** and **2** have been calculated by use of eq 1 for solutions of different polarity, that is, toluene ($\epsilon_s = 2.38$), chlorobenzene ($\epsilon_s = 5.72$), THF ($\epsilon_s = 7.51$), and *o*-dichlorobenzene ($\epsilon_s = 9.93$) (Table 2). The radius of the $PERY^{-\bullet}$ radical anion was set to $r^- = 4.7$ Å[9] and those of the $OPV^{+\bullet}$ and $OAn^{+\bullet}$ radical cations to $r^+ = 5.5$[25] and 4.8 Å,[22] respectively. The R_{cc} distances have been determined from molecular modeling, with the assumption that the charges are located at the center of the OAn, OPV, and PERY moieties. For **1** these are $R_{cc} = 21$ Å for $OPV^{+\bullet}$–$PERY^{-\bullet}$ and $R_{cc} = 41$ Å for $OAn^{+\bullet}$–OPV–$PERY^{-\bullet}$.[26] For **2**, the orientation and distance between OAn–OPV and PERY units is not fixed owing to the flexible spacer. The upper limit for the R_{cc} distance in **2** has been determined in a conformation in which all chromophores are coplanar, resulting in $R_{cc} = 27$ Å for $OPV^{+\bullet}$–$PERY^{-\bullet}$ and $R_{cc} = 44$ Å for $OAn^{+\bullet}$–OPV–$PERY^{-\bullet}$.

Table 2 shows that photoinduced charge separation, charge shift, and charge recombination (CS1, CSH1, CR1, and CR2) are exergonic for arrays **1** and **2** in all solvents, with the exception that the driving force for charge shift is close to zero in toluene. Similar energy values are obtained for both arrays, because they essentially differ only in the value of R_{cc}.

Photoluminescence in Solution. Photoluminescence (PL) spectroscopy was used to investigate the photoinduced energy and electron-transfer reactions in **1** and **2** qualitatively. The OPV fluorescence of **1** in toluene at 519 nm is quenched by a factor $Q = 50$ compared to that of the OPV model compound after photoexcitation at 400 nm (Figure 4). Also, the PERY fluorescence of **1** at 540 nm is quenched ($Q = 3000$) with respect to the PERY model (Figure 4b) after selective excitation at 530 nm. The excitation spectra of the residual luminescence at 519 and 540 nm do not fully superimpose with the absorption spectrum of **1** but coincide with the absorption spectrum of the OAn and OPV chromophores only (Figure 4a). This suggests that energy transfer (ET1) occurs from the OAn to the OPV segment. The fact that the excitation spectra do not show a PERY feature is tentatively explained by a small OAn–OPV contamination, not linked to a PERY chromophore. The negligible residual fluorescence of the PERY chromophore of **1** indicates that the quantum yield for charge separation to the OAn–$OPV^{+\bullet}$–$PERY^{-\bullet}$–OPV–OAn state is close to unity. Similar quenching factors have been measured in solvents of higher polarity (e.g., THF and *o*-dichlorobenzene), indicating that charge separation is similarly fast.

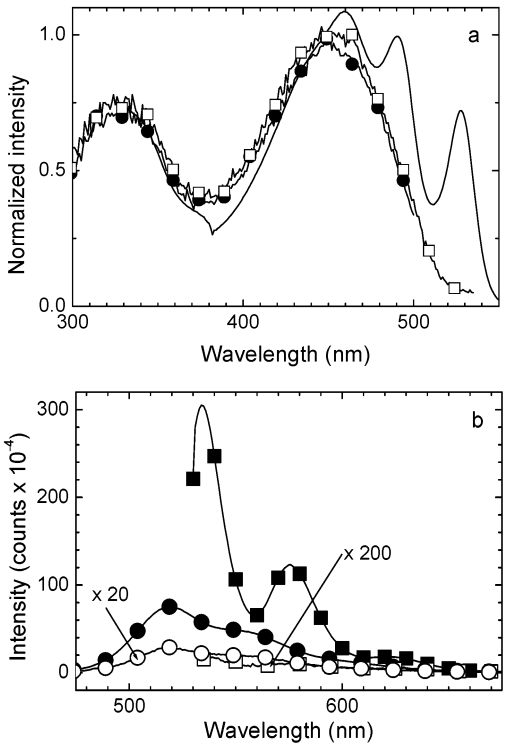

Figure 4. (a) Absorption (—) and excitation spectra of the 519 (●) and 540 nm fluorescence (□) of **1** in toluene solution. (b) Fluorescence spectra of the OPV (●) and PERY (■) reference compounds and of **1** in toluene after selective excitation of the OPV (○) and the PERY (□) chromophores at 400 and 530 nm.

For investigating the photophysics of **2** we used solvents (e.g., THF) in which aggregation does not occur. In THF the fluorescence of the OPV and PERY chromophores of **2** is quenched, with quenching factors of $Q = 66$ and 300, respectively (Figure 5). The excitation spectra of the residual OPV and PERY emission coincide with the absorption spectrum of **2**, consistent with a multistep energy transfer process (ET1 and ET2) to the lowest singlet excited state. The emission of the PERY chromophore in **2** is 10 times more intense than in **1**. This result suggests that the charge separation process (CS1) is slower in **2**, as a result of the saturated spacer between OPV and PERY units. Because the residual emission is similar with excitation at 400 and 530 nm, and the excitation spectrum reflects the features of all three chromophores, we conclude that the sample of **2** does not contain the small OAn–OPV contamination likely present in **1**.

Transient Absorption Spectroscopy. To monitor the photophysical processes in more detail, transient absorption spectroscopy has been performed in the subpicosecond to nanosecond time domain. Subpicosecond experiments on **1** and **2** were

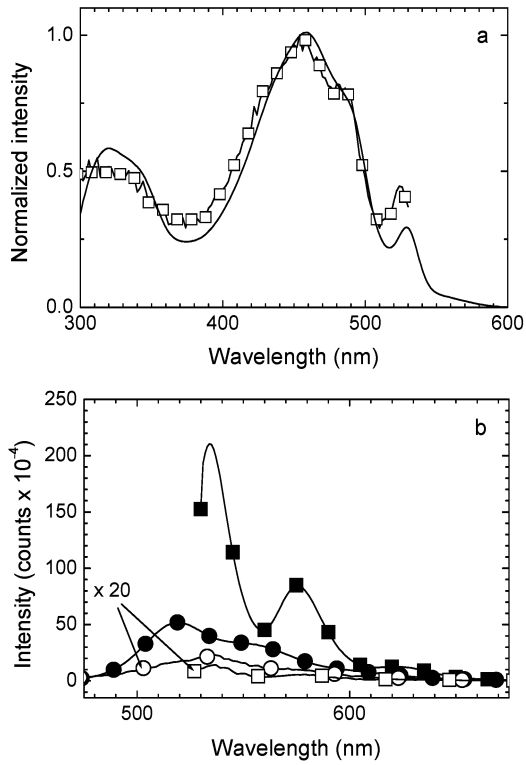

Figure 5. (a) Absorption (solid line) and excitation of the 534 nm emission (□) spectra of **2** in THF solution. (b) Fluorescence spectra of the OPV (●) and PERY (■) reference compounds and of **2** in THF after selective excitation of the OPV (○) and the PERY (□) chromophores at 400 and 530 nm.

performed by selective excitation of the OPV or PERY chromophores at 455 or 520 nm with ∼150 fs pulses, while the transient differential transmission at 1450, 900, and 700 nm was monitored. The absorption at 1450 nm is highly characteristic for the low-energy transition of the $OPV^{+\bullet}$ radical cation,[25] and hence, this transient signal gives direct information on the rates of formation (CS1 or CS2) and decay (CR1 and CSH1) of the OAn−$OPV^{+\bullet}$−$PERY^{-\bullet}$−OPV−OAn charge-separated state. At 700 nm, the radical ions of all chromophores absorb, with molar absorption coefficients of 7×10^3, 15×10^3, and $\sim 80 \times 10^3$ M^{-1} cm^{-1} for $OAn^{+\bullet}$, $OPV^{+\bullet}$,[27] and $PERY^{-\bullet}$,[28] respectively. Therefore, the 700 nm absorption indicates the presence of both the OAn−$OPV^{+\bullet}$−$PERY^{-\bullet}$−OPV−OAn and $OAn^{+\bullet}$−OPV−$PERY^{-\bullet}$−OPV−OAn charge-separated states.[27,28] Finally, at 900 nm the ^{1}OPV* and ^{1}PERY* singlet states dominate the transient absorption. At this wavelength the radical ions absorb as well, though with much lower molar absorption coefficients than at 700 nm.

Array 1 in Toluene. The transient differential transmission of **1** in toluene at 1450 nm (associated with the $OPV^{+\bullet}$ radical cation band of the OAn−$OPV^{+\bullet}$−$PERY^{-\bullet}$−OPV−OAn charge-separated state) of **1** in toluene exhibits a fast rise and a slow decrease after excitation at 450 nm (Figure 6). The rise occurs within 1 ps. This high rate for charge separation ($k_{CS1} > 1000$ ns^{-1}, Table 2) is in agreement with the near-complete quenching of the PERY emission (Figure 4b). The charge-separated state can evolve directly from the ^{1}OPV* singlet excited state (CS2) or, via an intermediate energy transfer (ET2), from the ^{1}PERY* singlet excited state (CS1). Since the rate of formation of $OPV^{+\bullet}$ was independent of the excitation wavelength, 450 nm (OPV) or 520 nm (PERY), we favor the latter interpretation.[29] The slow decay of the 1450 nm absorption reveals that the OAn−$OPV^{+\bullet}$−$PERY^{-\bullet}$−OPV−OAn charge-separated state has a

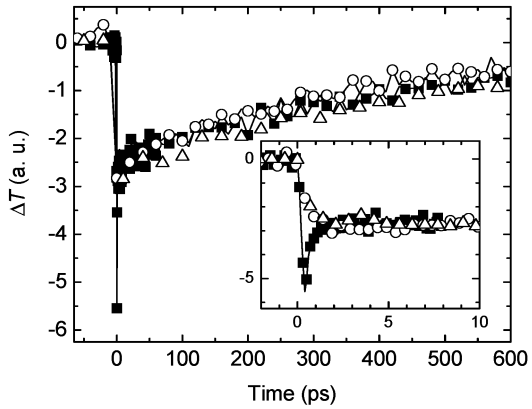

Figure 6. Differential transmission dynamics of **1** in toluene monitored at 1450 (○), 900 nm (■), and 700 (△) with excitation at 450 nm. The inset shows the differential transmissions at shorter time delays.

rather long lifetime (∼370 ps) in toluene. The transient absorption of the $PERY^{-\bullet}$ radical anion in **1**, recorded at 700 nm, essentially superimposes with the temporal evolution of the band at 1450 nm (Figure 6). This confirms that both absorptions originate from the same charged species, that is, OAn−$OPV^{+\bullet}$−$PERY^{-\bullet}$−OPV−OAn, and that no charge shift occurs in toluene. The differential transmission at 900 nm (^{1}OPV* or ^{1}PERY*) exhibits an abrupt rise and decay in the first picosecond, corresponding to the formation and decay of the ^{1}OPV* (or ^{1}PERY*) singlet-excited state (Figure 6). A similar signal is observed when the pump pulse is shifted from 450 to 520 nm to excite the PERY chromophore. The ^{1}OPV* and ^{1}PERY* states evolve within 1 ps into the OAn−$OPV^{+\bullet}$−$PERY^{-\bullet}$−OPV−OAn charge-separated state, as evidenced by the 1450 and 700 nm transient absorptions. In accordance, the signal at 900 nm exhibits the same temporal evolution as the 1450 and 700 nm differential transmissions after the initial transient singlet state feature has decayed.

Array 1 in Polar Solvents. In more polar media than toluene, the OAn−$OPV^{+\bullet}$−$PERY^{-\bullet}$−OPV−OAn → $OAn^{+\bullet}$−OPV−$PERY^{-\bullet}$−OPV−OAn charge shift (CSH1) is exergonic for **1** (Table 2). The differential transmission of the $OPV^{+\bullet}$ radical cation (at 1450 nm) shows that charge separation to the OAn−$OPV^{+\bullet}$−$PERY^{-\bullet}$−OPV−OAn state of **1** dissolved in THF also occurs with a high rate ($k_{CS} > 1000$ ns^{-1}) but that, compared to toluene, the lifetime of this state is dramatically reduced (12 vs 370 ps) (Figure 7). The same kinetics was observed with excitation at 450 (OPV) or 520 nm (PERY). The differential transmission at 700 nm of the $PERY^{-\bullet}$ radical anion in array **1** in THF reveals the existence of two different time regimes (Figure 7). The first region exhibits a fast rise and decay during the first 30 ps. This initial feature is associated with the formation and decay of the OAn−$OPV^{+\bullet}$−$PERY^{-\bullet}$−OPV−OAn state and both $OPV^{+\bullet}$ and $PERY^{-\bullet}$ radical ions account for the transient absorption at 700 nm. After 30 ps, most of the signal has decayed and a less intense, long-lived signal remains, which constitutes the second regime. Because the $OPV^{+\bullet}$ absorption at 1450 nm has disappeared after 30 ps, the long-lived signal at 700 nm is attributed to the $OAn^{+\bullet}$−OPV−$PERY^{-\bullet}$−OPV−OAn charge-separated state, formed by an intramolecular redox reaction of the primary charge-separated state. The differential transmission of **1** in THF at 900 nm exhibits the formation and decay of the singlet-excited state of the OPV and PERY chromophores (depending on which has been excited) in the first picosecond after photoexcitation (Figure 7). As in toluene, the singlet-excited state is quenched by charge separation to OAn−$OPV^{+\bullet}$−$PERY^{-\bullet}$−OPV−OAn. After 20

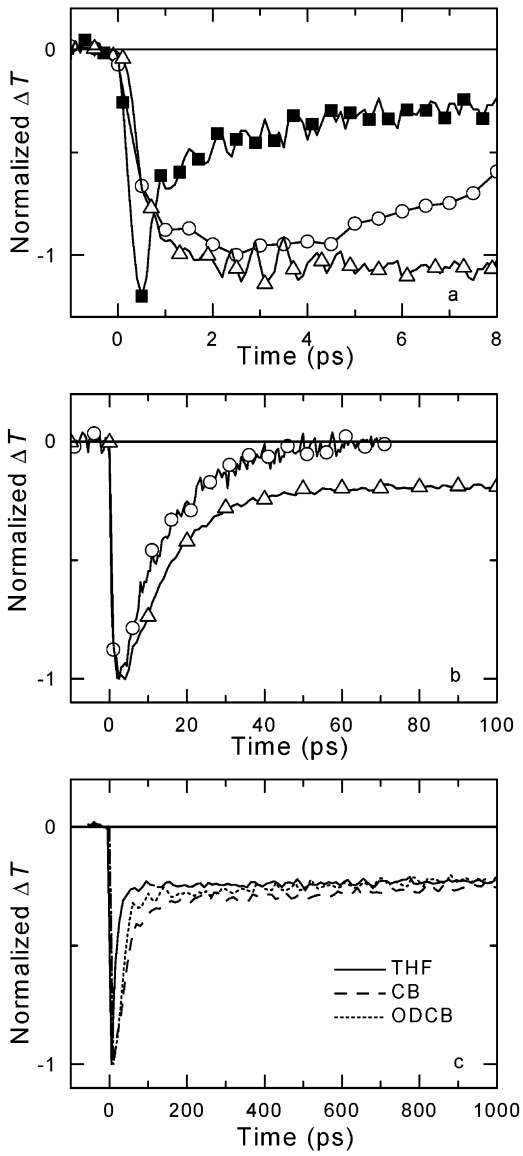

Figure 7. Differential transmission dynamics of **1** in THF monitored at 1450 (○), 900 (■), and 700 nm (△) with excitation at 450 nm, measured at different time delays. Panel c shows the 700 nm data obtained for **1** in THF, chlorobenzene, and *o*-dichlorobenzene.

ps, an almost constant signal remains, corresponding to the $OAn^{+\bullet}{}^{-}OPV-PERY^{-\bullet}-OPV-OAn$ state.

Even though the rate for the charge shift (CSH1) cannot be extracted from the data, an efficiency of 0.22 (±0.02) in THF can be estimated from the transient absorption at 700 nm, by using the molar absorption coefficients of the involved radical ions at this wavelength and assuming that the maximum intensity at 3 ps corresponds to the $OAn-OPV^{+\bullet}-PERY^{-\bullet}-OPV-OAn$ state, while at 50 ps the remaining absorption corresponds to the $OAn^{+\bullet}-OPV-PERY^{-\bullet}-OPV-OAn$ state only. In chlorobenzene and *o*-dichlorobenzene, solvents of lower and higher polarity than THF, the differential transmissions at 1450, 900, and 700 nm of **1** exhibit similar time profiles as those observed in THF. The efficiencies for charge shift are similar in all the polar solvents (Figure 7c).

Because the 700 nm signal of the $OAn^{+\bullet}-OPV-PERY^{-\bullet}-OPV-OAn$ state does not decay within the first nanoscond (Figure 7c), we used nanosecond transient spectroscopy to obtain information on rate of charge recombination (CR2). Figure 8a shows the transient spectra in the 480−850 nm region obtained

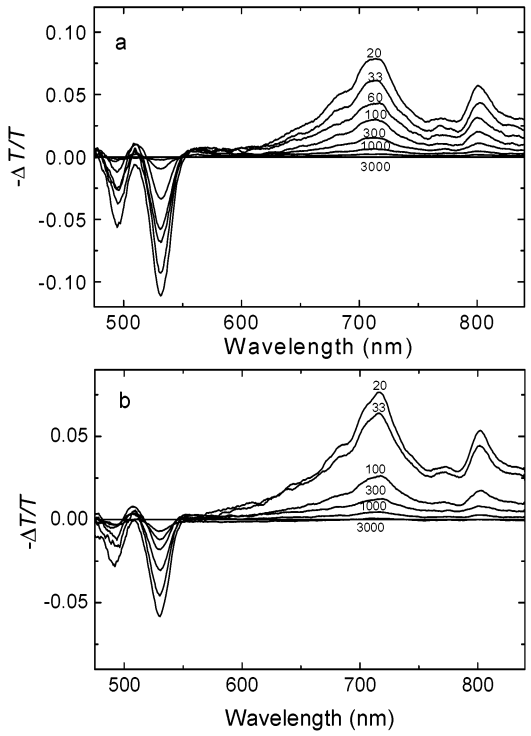

Figure 8. Differential transmission of (a) **1** and (b) **2** in *o*-dichlorobenzene solution (5×10^{-5} M), measured at room temperature with photoexcitation at 450 nm with 4 ns pulses. The absorption bands of the $PERY^{-\bullet}$ radical anion can be observed at 710 and 800 nm. The numbers indicate the time delay in nanoseconds after the excitation pulse.

after excitation of **1** in ODCB with a 4 ns pulse at 450 nm. The spectra show the well-defined absorption features corresponding to the $PERY^{-\bullet}$ radical anion at 710 and 800 nm and the associated bleaching in the visible range at 495 and 532 nm. The absorption of the $OAn^{+\bullet}$ radical cation cannot be clearly distinguished because its electronic transitions overlap with those of the $PERY^{-\bullet}$ radical anion and are less intense [ϵ(860 nm) ≈ 15×10^3 M^{-1} cm^{-1} for $OAn^{+\bullet}$ vs ϵ(800 nm) ≈ 60×10^3 M^{-1} cm^{-1} for $PERY^{-\bullet}$]. The signals can be observed into the microsecond time domain and demonstrate the longevity of the $OAn^{+\bullet}-OPV-PERY^{-\bullet}-OPV-OAn$ state. The decay of the signals under these conditions does not follow first-order kinetics, and hence it is not possible to determine a monomolecular lifetime. This observation is consistent with the fact that at the concentration used (5×10^{-5} M) the lifetime of the charge-separated state is much longer than the average time between diffusion-limited collisions, which is on the order of ∼40 ns.

Array 2 in Polar Solvents. In THF, the rate for intramolecular photoinduced charge separation in **2** ($k_{CS1} = 285$ ns^{-1}) is less than in **1** ($k_{CS1} = 1000$ ns^{-1}) as evidenced by the slower grow-in of the differential transmission at 1450 nm of the $OAn-OPV^{+\bullet}-PERY^{-\bullet}-OPV-OAn$ state (Figure 9). The reduced rate constant is consistent with the smaller quenching of the PERY fluorescence of **2** compared to **1** and likely is attributed to a smaller electronic coupling between OPV donor and PERY acceptor in the excited state. Likewise, the rate for charge recombination has decreased in **2**, giving the primary charge-separated state in **2** a longer lifetime (100 ps) than in **1** (12 ps). The efficiency of the intramolecular charge shift generating the $OAn^{+\bullet}-OPV-PERY^{-\bullet}-OPV-OAn$ state in **2** has increased to 0.28 (±0.03), as inferred from the transient absorption at 700 nm (Figure 9). Similar to **1**, the efficiency for the charge

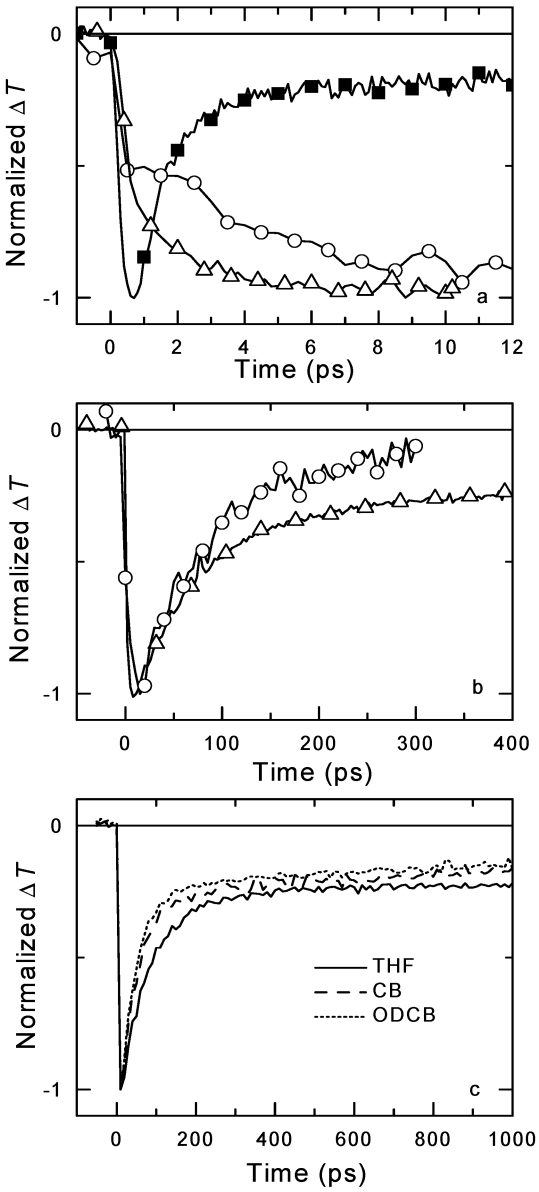

Figure 9. Differential transmission dynamics of **2** in THF monitored at 1450 (○), 900 (■), and 700 nm (△) with excitation at 455 nm, measured at different time delays. Panel c shows 700 nm data obtained for **2** in THF, chlorobenzene, and *o*-dichlorobenzene.

shift in **2** is only weakly dependent on the solvent (THF, chlorobenzene, or *o*-dichlorobenzene; Figure 9c) and the $OAn^{+}\bullet-OPV-PERY^{-}\bullet-OPV-OAn$ persists in solution into the microsecond domain.

Discussion

Marcus theory provides an estimate for the energy barrier ($\Delta G^{\ddagger}$) for electron transfer based on the change in energy ($\Delta G°$) and the reorganization energy (λ) via[30]

$$\Delta G^{\ddagger} = \frac{(\Delta G° + \lambda)^2}{4\lambda} \qquad (2)$$

The reorganization energy consists of an internal contribution (λ_i) and a solvent term (λ_s), which can be approximated via the Born−Hush approach to give after summation, with n the index of refraction:[31]

$$\lambda = \lambda_i + \lambda_s = \lambda_i + \frac{e^2}{4\pi\epsilon_0}\left(\frac{1}{2}\left(\frac{1}{r^+} + \frac{1}{r^-}\right) - \frac{1}{R_{cc}}\right)\left(\frac{1}{n^2} - \frac{1}{\epsilon_s}\right) \qquad (3)$$

The rate constants for the different processes (Table 2) are a function not only of the energy barrier $\Delta G^{\ddagger}$ but also of the reorganization energy (λ) and the electronic coupling (V) between donor and acceptor in the excited state, according to[32]

$$k = \left(\frac{4\pi^2}{h^2\lambda k_B T}\right)^{1/2} V^2 \exp\left[-\frac{(\Delta G° + \lambda)^2}{4\lambda k_B T}\right] \qquad (4)$$

The values of $\Delta G°$, λ, and $\Delta G^{\ddagger}$ calculated from eqs 1−3 are collected in Table 3. The initial charge separation (CS1) occurs close to the Marcus optimal region because $-\Delta G°$ and λ are similar, and hence $\Delta G^{\ddagger} \approx 0$. In such a situation, the reaction rate is governed by the electronic coupling V between the donor and acceptor and the polarity of the solvent becomes less important. The electronic coupling depends on the nature of the spacer and on the separation of donor and acceptor via $V^2 = V_0^2(R_0)\exp[-\beta(R_{cc} - R_0)]$, with R_0 the contact distance. The electronic coupling in array **1** is likely high due to the short distance between the OPV and the PERY chromophores, although the frontier molecular orbitals of the perylene diimide have nodes at the imide nitrogen and direct conjugation is absent. The strong coupling explains the high rate constants for charge separation in **1** in all solvents ($k_{CS1} > 1000\ ns^{-1}$). In contrast, charge recombination (CR1) in $OAn-OPV^{+}\bullet-PERY^{-}\bullet-OPV-OAn$ is in the Marcus inverted region ($-\Delta G° > \lambda$) for all solvents (Table 3), and consequently, the barrier for charge recombination reduces with solvent polarity. In toluene, the most apolar solvent used, the energy barrier for the recombination is remarkably high, and consistently a rather long lifetime (370 ps) of the $OAn-OPV^{+}\bullet-PERY^{-}\bullet-OPV-OAn$ charge-separated state has been observed. In the more polar solvents, the calculated energy barrier is significantly less and recombination is expected to be much faster. This explains, to some extent, the 12 ps lifetime of the $OAn-OPV^{+}\bullet-PERY^{-}\bullet-OPV-OAn$ charge-separated state in THF.

The charge shift occurs in the normal region ($-\Delta G° < \lambda$) and is energetically less favorable than charge recombination

TABLE 3: Change in Gibbs Energy ($\Delta G°$)[a]

		array **1**			array **2**		
reaction[b]	solvent	$\Delta G°$ (eV)	λ (eV)	$\Delta G^{\ddagger}$ (eV)	$\Delta G°$ (eV)	λ (eV)	$\Delta G^{\ddagger}$ (eV)
CS1	TOL	−0.45	0.36	0.006	−0.34	0.36	0.000
	CB	−0.98	0.85	0.005	−0.90	0.89	0.000
	THF	−1.07	0.94	0.004	−1.00	0.99	0.000
	ODCB	−1.14	0.98	0.007	−1.08	1.03	0.001
CR1	TOL	−1.88	0.36	1.625	−1.99	0.36	1.846
	CB	−1.35	0.85	0.072	−1.43	0.89	0.080
	THF	−1.26	0.94	0.026	−1.33	0.99	0.029
	ODCB	−1.19	0.98	0.011	−1.25	1.03	0.013
CSH1	TOL	−0.03	0.35	0.073	−0.06	0.35	0.060
	CB	−0.16	0.83	0.135	−0.16	0.83	0.135
	THF	−0.18	0.92	0.148	−0.18	0.83	0.128
	ODCB	−0.20	0.95	0.149	−0.19	0.95	0.152
CR2	TOL	−1.85	0.37	1.474	−1.93	0.37	1.636
	CB	−1.19	0.98	0.011	−1.26	0.99	0.019
	THF	−1.08	1.10	0.000	−1.15	1.11	0.000
	ODCB	−0.99	1.18	0.008	−1.06	0.99	0.001

[a] With reference to the lowest singlet excited state, reorganization energy (λ), and barrier ($\Delta G^{\ddagger}$), determined by use of eqs 1−3. [b] For definitions see Figure 3.

(Table 3). Consequently, the energy barrier is higher. These two facts rationalize that the charge shift is slower than the charge recombination, although the actual rates will also strongly depend on the electronic coupling *V*, which is not accounted for in this analysis. In a study on a related system with C_{60} as an acceptor instead of perylene diimide, (OAn−OPV−C_{60}),[22] we have shown recently that increasing the lifetime of the primary charge-separated state is beneficial for the slower charge shift process to compete. In principle this condition is nicely fulfilled for array **1** in toluene, but here the driving force for the charge shift is close to zero and the charge shift does not occur. Nevertheless, in polar solvents, where charge recombination is accelerated, the charge shift can be observed. The efficiency of the charge shift is similar in all polar solvents, consistent with the small variation in energy barriers for the charge shift (Table 3).

The rate for charge separation (CS1) is smaller for **2** than for **1**, despite the similarly low energy barrier (Table 3). The reason for this difference is the type of linker between PERY and OPV units. In **2,** electron transfer must occur over a longer distance, through space or through the saturated spacer by a superexchange mechanism, resulting in a reduced electronic coupling. The same effect occurs in the charge recombination and explains the longer lifetime of the OAn−$OPV^{+\bullet}$−$PERY^{-\bullet}$−OPV−OAn state of **2** in THF (100 ps) compared to that of **1** (12 ps). We assume that slower charge recombination increases the efficiency for the charge shift in **2** with respect to **1**.

For both **1** and **2**, the product of the charge shift, $OAn^{+\bullet}$−OPV−$PERY^{-\bullet}$−OPV−OAn, has a long lifetime, even though the charge recombination from this state (CR2) is almost barrierless (Table 3). The explanation for the longevity is that the large distance between the $OAn^{+\bullet}$ and the $PERY^{-\bullet}$ redox sites reduces their electronic coupling and hampers charge recombination (CR2) from the $OAn^{+\bullet}$−OPV−$PERY^{-\bullet}$−OPV−OAn state, resulting in a long lifetime.

Conclusions

Two multichromophoric arrays **1** and **2** have been synthesized by covalently linking OAn, OPV, and PERY chromophores into a symmetrical OAn−OPV−PERY−OPV−OAn configuration. The UV−visible absorption spectra demonstrate that the chromophores are essentially electronically decoupled. There is some indication that the OAn−OPV and PERY chromophores are in close proximity in **2** and that this structure is essentially backfolded (a situation that cannot occur in **1)**. Sequential photoinduced intramolecular charge separation occurs in both multichromophoric arrays. The electron-transfer reactions start with the formation of the primary OAn−$OPV^{+\bullet}$−$PERY^{-\bullet}$−OPV−OAn charge-separated state. The rate for initial charge separation is independent of the chromophore (OPV or PERY) that is excited. This indicates that charge separation originates from the ^{1}PERY* state—that is, CS1 rather than CS2 (Figure 3)—and that it is preceded by an ultrafast ^{1}OPV → ^{1}PERY* energy transfer (ET1) if the OPV is excited initially. The primary charge-separated state decays via charge recombination (CR1) or produces the secondary, more stable $OAn^{+\bullet}$−OPV−$PERY^{-\bullet}$−OPV−OAn charge-separated state via an intramolecular redox reaction or charge shift (CSH1).

Regardless of the polarity of the solvent, the intramolecular charge separation is extremely fast in **1**, because it occurs in the optimal region ($-\Delta G^\circ \sim \lambda$). Charge recombination occurs in the Marcus inverted region ($-\Delta G^\circ > \lambda$) and is fast in polar solvents but remarkably slow in toluene. Both charge separation and recombination are slowed in **2**, because the saturated spacer reduces the electronic coupling between the OPV donor and PERY acceptor in the excited state, possibly also due to backfolding.

The charge shift that generates the $OAn^{+\bullet}$−OPV−$PERY^{-\bullet}$−OPV−OAn state competes with charge recombination and occurs in THF with an efficiency of 0.22 for **1** and 0.28 for **2**. The higher efficiency for **2** is ascribed to the reduced rate constant for charge recombination from the primary charge-separated state in **2**. Compared to the lifetime of the $OPV^{+\bullet}$−$PERY^{-\bullet}$−OPV charge-separated state in triads (11 ps in THF),[6] the more stable $OAn^{+\bullet}$−OPV−$PERY^{-\bullet}$−OPV−OAn state has a lifetime that is many orders of magnitude longer, as it can be observed into the microsecond domain in THF at room temperature.

Experimental Section

All reagents and solvents were used as received or purified by standard procedures. NMR spectra were recorded on a Varian Mercury Vx at frequencies of 400 and 100 MHz for ^{1}H and ^{13}C nuclei or Varian Gemini 2000 at frequencies of 300 and 75 MHz for ^{1}H and ^{13}C nuclei, respectively. Fourier transform infrared (FT-IR) spectra were recorded on a Perkin-Elmer Spectrum One UATR FT-IR. Elemental analyses were preformed on a Perkin-Elmer 2400 series II CHN Analyzer. Matrix-assisted laser desorption ionization time-of-flight mass spectrometry (MALDI-TOF MS) was performed on a Perseptive DE PRO Voyager MALDI-TOF mass spectrometer with a dithranol matrix. A Shimadzu LC-10AT system combined with a Polymer Laboratories MIXED-D column (particle size 5 μm; length/i.d. 300 mm × 7.5 mm) and UV detection was employed for size-exclusion chromatography (SEC), with $CHCl_3$ as an eluent (1 mL/min).

Diethyl (4-Nitrobenzyl) Phosphonate (4). Triethyl phosphite (2.30 g, 13.88 mmol) and 4-nitrobenzyl bromide (2 g, 9.25 mmol) were heated to 160 °C and stirred for 2 h. Subsequently, the mixture was cooled to 70 °C and the formed ethyl bromide and excess triethyl phosphite were distilled under reduced pressure. The residue was dissolved in ethyl acetate and filtered over silica gel. The solvent was removed in vacuo to yield 2.2 g of diethyl 4-nitrobenzyl phosphonate. ^{1}H NMR ($CDCl_3$, 300 MHz) δ 8.18 (d, 2H), 7.5 (d, 2H), 4.07 (m, 4H), 3.27 (d, 2H), 1.28 (t, 6H); ^{13}C NMR ($CDCl_3$, 75 MHz) δ 146.78, 139.62 (d), 130.45(d), 123.44 (d), 62.20 (d), 34.61, 32.79, 16.15 (d).

(*E*,*E*,*E*,*E*)-4-[4-[4-{4-[*N*-(4-(Diphenylamino)phenyl)-(*N*-phenyl-3-aminostyryl)]-2,5-bis[(*S*)-2-methylbutoxy]styryl]-2,5-bis[(*S*)-2-methylbutoxy]styryl}-2,5-bis[(*S*)-2-methylbutoxy]-styryl]nitrobenzene (5). Diethyl 4-nitrobenzyl phosphonate (73 mg, 0.27 mmol), was dissolved in anhydrous dimethylformamide (DMF) (6 mL) under an argon atmosphere, and K*t*BuO (35 mg, 0.32 mmol) was added to the solution at room temperature. After 15 min a solution of aldehyde **3** (307 mg, 0.243 mmol) in 3 mL of DMF/THF (2/1) was added dropwise to the reaction mixture. Twenty minutes after the addition was completed, the product started precipitating from solution. The reaction mixture was stirred for 2 h more. The product was isolated by filtration, washed with ethanol and methanol, and obtained as a red powder (0.290 g, 86%). ^{1}H NMR ($CDCl_3$, 300 MHz) δ 8.22 (d, 2H), 7.65 (d, 1H), 7.63 (d, 2H), 7.57 (d, 1H), 7.52 (s, 2H), 7.51 (d, 1H), 7.40 (d, 1H), 7.31−6.96 (m, 31H), 4.05−3.72 (m, 12H), 2.10−1.85 (m, 6H), 1.70−1.45 (m, 6H), 1.45−1.2 (m, 6H), 1.2−0.85 (m, 36H); ^{13}C NMR ($CDCl_3$, 75 MHz) δ 151.81, 151.25, 151.01, 148.21, 147.84, 146.43, 144.73, 142.90, 142.70, 139.15, 129.45, 129.18, 128.42, 128.31, 127.75, 127.59, 127.07, 126.63, 126.04, 125.45, 125.30, 125.11,

124.18, 123.78, 122.96, 122.79, 122.68, 122.42, 122.24, 120.29, 111.15, 110.67, 110.01, 109.89, 109.70, 109.53, 74.47, 74.25, 74.16, 74.04, 73.94, 35.13, 35.05, 34.94, 26.37, 16.85, 11.52, 11.38. MALDI-TOF MS (MW = 1382.87) m/z = 1382.0 $[M]^+$; Anal. Calcd for $C_{92}H_{107}N_3O_8$: C, 79.9; H, 7.8; N, 3.0. Found: C, 79.7; H, 7.8; N, 2.7.

(*E*,*E*,*E*,*E*)-4-[4-[4-{4-[*N*-(4-(Diphenylamino)phenyl)-(*N*-phenyl-3-aminostyryl)]-2,5-bis[(*S*)-2-methylbutoxy]styryl]-2,5-bis[(*S*)-2-methylbutoxy]styryl}-2,5-bis[(*S*)-2-methylbutoxy]-styryl]aniline (6). Under an Ar atmosphere, nitro compound **5** (0.28 g, 0.2 mmol) was suspended in EtOAc (15 mL). $SnCl_2 \cdot H_2O$ (0.36 g, 1.62 mmol) was added and the mixture was heated to 85 °C, before EtOH (2 mL) was added. The reaction mixture was stirred for 5 h at 95 °C and subsequently cooled to room temperature. After being cooled to room temperature, the reaction mixture was poured into crushed ice. The aqueous phase was slightly basified by the addition of 0.1 M NaOH and was subsequently extracted three times with diethyl ether. The collected organic fractions were dried over $MgSO_4$, and the solvent was removed in vacuo. Purification by column chromatography (silica gel, pentane/CH_2Cl_2 1:1, R_f = 0.4), yielded **6** (0.19 g, 70%) as an orange solid. ^{1}H NMR ($CDCl_3$, 400 MHz) δ 7.52 (s, 4H), 7.42 (d, 1H), 7.36 (d, 2H), 7.31 (d, 1H), 7.27−6.97 (m, 31H), 6.69 (d, 2H), 3.93−3.89 (m, 12H), 1.70−1.45 (m, 6H), 1.45−1.2 (m, 6H), 1.2−0.85 (m, 36H); ^{13}C NMR ($CDCl_3$, 75 MHz) δ 151.23, 151.08, 151.02, 150.95, 148.17, 147.81, 145.94, 142.86, 142.69, 139.15, 129.43, 129.17, 128.77, 128.67, 128.30, 127.72, 127.53, 127.36, 127.21, 126.79, 126.43, 125.44, 125.30, 123.77, 123.71, 123.59, 122.68, 122.41, 122.25, 120.26, 119.88, 115.22, 110.62, 110.41, 109.85, 109.65, 74.44, 74.28, 74.06, 73.99, 35.13, 35.04, 34.98, 34.92, 26.37, 26.29, 16.89, 16.87, 16.82, 16.79, 11.54, 11.48, 11.41, 11.37. MALDI-TOF MS (MW = 1352.89) m/z = 1352.92 $[M]^+$.

***N*,*N*′-Bis[(*E*,*E*,*E*,*E*)-4-[4-[4-{4-[*N*-(4-(Diphenylamino)phenyl)-(*N*-phenyl-3-aminostyryl)]-2,5-bis[(*S*)-2-methylbutoxy]-styryl]-2,5-bis[(*S*)-2-methylbutoxy]styryl}-2,5-bis[(*S*)-2-methylbutoxy]styryl]phenyl]-3,4:9,10-perylenebis(dicarboximide) (1).** Amine **6** (55 mg, 0.04 mmol), 3,4:9,10-perylenetetracarboxylic dianhydride (8 mg, 0.02 mmol), imidazole (0.5 g, 7.3 mmol), and a catalytic amount of $Zn(AcO)_2$ were mixed and heated to 160 °C. After stirring for 4 h, the reaction mixture was cooled to room temperature. The residue was purified by column chromatography (silica gel, ethyl acetate/$CHCl_3$ 1:0−1:4, R_f = 0−0.4) and repetitive preparative size-exclusion chromatography (Bio Beads S-X1 and S-X3, CH_2Cl_2) to yield 9 mg (15%) of **1** as a dark red solid. ^{1}H NMR (CD_2Cl_2, 400 MHz) δ 8.61−8.52 (m, 8H), 7.61 (d, 4H), 7.51−6.89 (m, 77H), 3.90−3.70 (m, 24H), 1.94−1.82 (m, 12H), 1.65−1.52 (m, 12H), 1.36−1.25 (m, 12H), 1.07−0.90 (m, 64H). MALDI-TOF MS (MW = 3062.08) m/z = 3060.64 $[M]^+$.

(*E*,*E*,*E*,*E*)-4-[4-[4-{4-[*N*-(4-(Diphenylamino)phenyl)-(*N*-phenyl-3-aminostyryl)]-2,5-bis[(*S*)-2-methylbutoxy]styryl]-2,5-bis[(*S*)-2-methylbutoxy]styryl}-2,5-bis[(*S*)-2-methylbutoxy]-styryl]phenylisocyanate (7). Amine **6** (50 mg, 0.04 mmol) was suspended in 20% phosgene solution in toluene (2.4 mL) and stirred at 95 °C for 16 h under an inert atmosphere. The reaction mixture was cooled to room temperature and the solvent was removed in vacuo. The complete conversion of the amine to the isocyanate was monitored by IR spectroscopy by observing the disappearance of the amine peak at 3364 cm^{-1} and the formation of the isocyanate peak at 2264 cm^{-1}. Compound **7** was used without further purification. MALDI-TOF MS (MW = 1378.91) m/z = 1378.64 $[M]^+$.

***N*,*N*′-Bis(1-isobutyl-2-hydroxyethyl)-3,4:9,10-perylenebis-(dicarboximide) (8).** (*S*)-(+)-Leucinol (0.455 g, 3.88 mmol), 3,4:9,10-perylenetetracarboxylic dianhydride (0.63 g, 1.61 mmol), imidazole (10 g), and catalytic amounts of $Zn(OAc)_2$ were heated to 160 °C and stirred for 1.5 h. After being cooled to room temperature, the reaction mixture was dissolved in dichloromethane, washed two times with 1 M HCl and brine, and dried over $MgSO_4$. The solvent was removed in vacuo to yield 0.72 g (75%) of a dark red solid. ^{1}H NMR (CD_2Cl_2, 400 MHz): δ 8.40−7.52 (m, 8H), 5.54−5.44 (br m, 2H), 4.60−4.48 (br m, 2H), 3.98−3.94 (m, 2H), 2.10−2.01 (m, 2H), 1.80−1.46 (br m, 4H), 1.10−0.92 (m, 12). MALDI-TOF MS (MW = 590.2) m/z = 590.1 $[M]^+$.

***N*,*N*′-Bis[1-isobutyl-2-[(*E*,*E*,*E*,*E*)-4-[4-[4-{4-[*N*-(4-(diphenylamino)phenyl)-(*N*-phenyl-3-aminostyryl)]-2,5-bis[(*S*)-2-methylbutoxy]styryl]-2,5-bis[(*S*)-2-methylbutoxy]styryl}-2,5-bis[(*S*)-2-methylbutoxy]styryl]phenylcarbamyl]ethyl]-3,4:9,10-perylenebis(dicarboximide) (2).** A solution of isocyanate **7** (38 mg, 0.027 mmol) in dry dichloromethane was added to a solution of **8** (7.4 mg, 0.012 mmol) in dry dichloromethane. Dibutylin dilaurate (3.22 mg) was added as a catalyst, and the reaction mixture was heated at reflux for 20 h under an argon atmosphere. The crude mixture was cooled to room temperature and the solvent was removed in vacuo. The residue was purified by silica gel chromatography (CH_2Cl_2/pentane 4:1, R_f = 0.15) and preparative size-exclusion chromatography (Bio Beads S-X3, CH_2Cl_2) to yield 20 mg (47%) of **2** as a red solid. ^{1}H NMR (CD_2Cl_2, 400 MHz) δ 9.38 (br s, 2H), 8.57, 8.21, 8.12, 7.79 (4d, 8H), 7.58−7.06 (m, 82H), 5.94−5.78 (br m, 2H), 5.35−5.18 (br m, 2H), 4.76−4.57 (br m, 2H), 3.98−3.83 (m, 24H), 2.37−2.22 (m, 2H), 2.02−1.89 (m, 14H), 1.75−1.60 (m, 16H), 1.52−1.32 (m, 12H), 1.16−0.99 (m, 84H); ^{13}C NMR (THF, 100 MHz) δ 165.00 (broad signal), 154.83, 153.07, 152.95, 150.14, 149.76, 144.83, 144.73, 141.33, 140.59, 136.06, 134.32, 132.50, 131.21, 131.09, 130.82, 130.60, 129.89, 129.79, 129.36, 129.18, 129.04, 128.89, 128.65, 128.34, 128.26, 127.74, 127.09, 126.99, 126.79, 126.79, 125.45, 125.06, 124.49, 124.37, 124.22, 124.12, 123.97, 123.28, 123.09, 121.83, 119.90, 112.15, 112.02, 111.47, 111.20, 111.13, 80.28, 75.64, 75.46, 53.07, 40.05, 37.07, 36.97, 36.89, 28.11, 27.26, 24.44, 23.65, 18.08, 12.73, 12.61. MALDI-TOF MS (MW = 3348.49) m/z = 3347.85 $[M]^+$.

Electrochemistry. Cyclic voltammograms were measured in 0.1 M tetrabutylammonium hexafluorophosphate ($TBAPF_6$) as a supporting electrolyte in dichloromethane (or THF) by use of a Potentioscan Wenking POS73 potentiostat. The working electrode was a Pt disk (0.2 cm^2), the counterelectrode was a Pt plate (0.5 cm^2), and a saturated calomel electrode (SCE) was used as reference electrode, calibrated against Fc/Fc^+ (+0.43 V).

Absorption and Photoluminescence. UV−visible−near-IR absorption spectra were recorded on a Perkin-Elmer Lambda 900 spectrophotometer. Fluorescence spectra were recorded on an Edinburgh Instruments FS920 double-monochromator spectrometer equipped with a Peltier-cooled red-sensitive photomultiplier.

Femtosecond Pump−Probe Spectroscopy. The femtosecond laser system used for pump−probe experiments consists of an amplified Ti/sapphire laser (Spectra Physics Hurricane). The single pulses from a continuous-wave mode-locked Ti/sapphire laser were amplified by a Nd:YLF laser by use of chirped pulse amplification, providing 150 fs pulses at 800 nm with an energy of 750 μJ and a repetition rate of 1 kHz. The pump pulses (450 or 520 nm) were created via optical parametric

amplification (OPA) of the 800 nm pulse by a BBO crystal into infrared pulses, which were then two times frequency-doubled via BBO crystals. The probe beam (700, 900, or 1450 nm) was generated in a separate optical parametric amplification setup. The pump beam was focused to a spot size of about 1 mm^2 with an excitation flux of 1 mJ cm^{-2} per pulse. For the 900 and 1450 nm probe pulses, a RG 850 nm cutoff filter was used to avoid contributions of residual probe light (800 nm) from the OPA. The probe beam was reduced in intensity compared to the pump beam by using neutral density filters of OD = 2. The pump beam was linearly polarized at the magic angle of 54.7° with respect to the probe, to cancel out orientation effects in the measured dynamics. The temporal evolution of the differential transmission was recorded on an Si or InGaAs detector by a standard lock-in technique at 500 Hz.

Nanosecond Pump−Probe Spectroscopy. Spectra were recorded by exciting the sample with pulses at 450 nm (pulse width 4 ns, repetition rate 10 Hz) obtained from an optical parametric oscillator (OPO), pumped by the third harmonic of a Nd:YAG laser. An intensified charge-coupled device (CCD) camera was used to record the transmission of a tungsten−halogen probe light through the sample after dispersion by a spectrograph. The signal acquisition by the CCD camera was electronically gated at different time delays after the excitation pulse, with a gate width of about a tenth of the delay time. To obtain differential transmission spectra, the reference transmission was recorded at a 20 ms delay.

Acknowledgment. This research has been supported by the Dutch Government through the E.E.T. program (EETK97115) and by The Netherlands Organization for Scientific Research (NWO) through a grant in the PIONIER program. The work of T.O. forms part of the research program of the Dutch Polymer Institute (DPI), project DPI324. The research of S.C.J.M. has been made possible by a fellowship of the Royal Netherlands Academy of Arts and Sciences.

References and Notes

(1) (a) *Molecular Electronics*; Jortner, J., Ratner, M., Eds.; Blackwell: London, 1997. (b) Lehn, J.-M. *Supramolecular Chemistry*; VCH: Weinheim, Germany, 1995. (c) *Electron Transfer in Chemistry*, Vol. I−IV; Balzani, V., Ed.; Wiley−VCH: Weinheim, Germany, 2001.

(2) For reviews see (a) Gust, D.; Moore, T. A.; Moore, A. L. *Acc. Chem. Res.* **1993**, *26*, 198. (b) Wasielewski, M. R. *Chem. Rev.* **1992**, *92*, 435. (c) Gust, D.; Moore, T. A.; Moore, A. L. *Acc. Chem. Res.* **2001**, *34*, 40. (d) Guldi, D. M. *Chem. Soc. Rev.* **2002**, *31*, 22. (e) Imahori, H.; Mori, Y.; Matano, J. *Photochem. Photobiol. C.* **2003**, *4*, 51.

(3) (a) Gust, D.; Moore, T. A.; Makings, L. R.; Liddell, P. A.; Nemeth, G. A.; Moore, A. L. *J. Am. Chem. Soc.* **1986**, *108*, 8028. (b) Sakata, Y.; Tatemitsu, H.; Bienvenue, E.; Seta, P. *Chem. Lett.* **1988**, 1625. (c) Collin, J. P.; Guillerez, S.; Sauvage, J.-P.; Barigelletti, F.; De Cola, L.; Flamigni, L.; Balzani, V. *Inorg. Chem.* **1991**, *30*, 4230. (d) Osuka, A.; Najata, T.; Maruyama, K.; Mataga, N.; Asahi, T.; Yamazaki, I.; Nishimura, Y. *Chem. Phys. Lett.* **1991**, *185*, 88. (e) Mecklenburg, S. L.; Peek, B. M.; Erickson, B. W.; Meyer, T. J. *J. Am. Chem. Soc.* **1991**, *113*, 8540. (f) Larson, S. L.; Cooley, L. F.; Elliott, C. M.; Kelley, D. F. *J. Am. Chem. Soc.* **1992**, *114*, 9504. (g) Brouwer, A. M.; Mout, R. D.; Maassen, P. H.; van den Brink, M.; van Ramesdonk, H. J.; Verhoeven, J. W.; Jonker, S. A.; Warman, J. M. *Chem. Phys. Lett.* **1991**, *186*, 481. (h) Brouwer, A. M.; Eijckelhoff, C.; Willemse, R. J.; Verhoeven, J. W.; Schuddeboom, W.; Warman, J. M. *J. Am. Chem. Soc.* **1993**, *115*, 2988. (i) Wasielewski, M. R.; Gaines, G. L., III; Wiederrecht, G. P.; Svec, W. A.; Niemczyk, M. P. *J. Am. Chem. Soc.* **1993**, *115*, 10442. (j) Gust, D.; Moore, T. A.; Moore, A. L. *J. Am. Chem. Soc.* **1993**, *115*, 11141. (k) Ohkohchi, M.; Takahasi, A.; Mataga, N.; Okada, T.; Osuka, A.; Yamada, H.; Maruyama, K. *J. Am. Chem. Soc.* **1993**, *115*, 12137. (l) Osuka, A.; Zhang, R. P.; Maruyama, K.; Ohno, T.; Nozaki, K. *Bull. Chem. Soc. Jpn.* **1993**, *66*, 3773. (m) Willemse, R. J.; Verhoeven, J. W.; Brouwer, A. M. *J. Phys. Chem.* **1995**, *99*, 5753. (n) Liddell, P. A.; Kuciauskas, D.; Sumida, J. P.; Nash, B.; Nguyen, D.; Moore, A. L.; Moore, T. A.; Gust, D. *J. Am. Chem. Soc.* **1997**, *119*, 1400. (o) Imahori, H.; Yamada, K.; Hasegawa, M.; Taniguchi, S.; Okada, T.; Sakata, Y. *Angew. Chem., Int. Ed. Engl.* **1997**, *36*, 2626. (p) Gosztola, D.; Niemczyk, M. P.; Wasielewski, M. R. *J. Am. Chem. Soc.* **1998**, *120*, 5118. (q) Kuciauskas, D.; Liddell, P. A.; Lin, S.; Johnson, T. E.; Weghorn, S. J.; Lindsey, J. S.; Moore, A. L.; Moore, T. A.; Gust, D. *J. Am. Chem. Soc.* **1999**, *121*, 8604. (r) Imahori, H.; Yamada, H.; Nishimura, Y.; Yamazaki, I.; Sakata, Y. *J. Phys. Chem. B* **2000**, *104*, 2099. (s) Miller, M. A.; Lammi, R. K.; Prathapan, S.; Holten, D.; Lindsey, J. S. *J. Org. Chem.* **2000**, *65*, 6634. (t) Hayes, R. T.; Wasielewski, M. R.; Gosztola, D. *J. Am. Chem. Soc.* **2000**, *122*, 5563. (u) Imahori, H.; Guldi, D. M.; Tamaki, K.; Yoshida, Y.; Luo, C.; Sakata, Y.; Fukuzumi, S. *J. Am. Chem. Soc.* **2001**, *123*, 6617. (v) Ambroise, A.; Kirmaier, C.; Wagner, R. W.; Loewe, R. S.; Bocian, D. F.; Holten, D.; Lindsey, J. S. *J. Org. Chem.* **2002**, *67*, 3811. (w) Sánchez, L.; Pérez, I.; Martín, N.; Guldi, D. M. *Chem. Eur. J.* **2003**, *9*, 2457. (x) Andersson, M.; Sinks, L. E.; Hayes, R. T.; Zhao, Y.; Wasielewski, M. R. *Angew. Chem., Int. Ed.* **2003**, *42*, 3139.

(4) (a) Sariciftci, N. S.; Smilowitz, L.; Heeger, A. J.; Wudl, F. *Science* **1992**, *258*, 1474. (b) Janssen, R. A. J.; Christiaans, M. P. T.; Hare, C.; Martín, N.; Sariciftci, N. S.; Heeger, A. J.; Wudl, F. *J. Chem. Phys.* **1995**, *103*, 8840.

(5) (a) Nogueira, A. F.; Montanari, I.; Nogueira, A. F.; Nelson, J.; Durrant, J. R.; Winder, C.; Loi, M. A.; Sariciftci, N. S.; Brabec, C. *J. Phys. Chem. B* **2003**, *107*, 1567. (b) Offermans, T.; Meskers, S. C. J.; Janssen, R. A. J. *J. Chem. Phys.* **2003**, *119*, 10924.

(6) Peeters, E.; van Hal, P. A.; Meskers, S. C. J.; Janssen, R. A. J.; Meijer, E. W. *Chem. Eur. J.* **2002**, *8*, 4470.

(7) Asha, S.: Schenning, A. P. H. J.; Meijer, E. W. *Chem. Eur. J.* **2002**, *8*, 3353.

(8) Schenning, A. P. H. J.; van Herrikhuyzen, J.; Jonkheijm, P.; Chen, Z.; Würthner, F.; Meijer, E. W. *J. Am. Chem. Soc.* **2002**, *124*, 10252.

(9) Neuteboom, E. E.; Meskers, S. C. J.; van Hal, P. A.; van Duren, J. K. J.; Meijer, E. W.; Dupin, H.; Pourtois, G.; Cornil, J.; Lazzaroni, R.; Brédas, J.-L.; Beljonne, D.; Janssen, R. A. J. *J. Am. Chem. Soc.* **2003**, *125*, 8625.

(10) Nierengarten, J.-F.; Eckert, J.-F.; Nicoud, J.-F.; Ouali, L.; Krasnikov, V.; Hadziioannou, G. *Chem. Commun.* **1999**, 617.

(11) Eckert, J.-F.; Nicoud, J.-F.; Nierengarten, J.-F.; Liu, S.-G.; Echegoyen, L.; Barigelletti, F.; Armaroli, N.; Ouali, L.; Krasnikov, V.; Hadziioannou, G. *J. Am. Chem. Soc.* **2000**, *122*, 7467.

(12) Peeters, E.; van Hal, P. A.; Knol, J.; Brabec, C. J.; Sariciftci, N. S.; Hummelen, J. C.; Janssen, R. A. J. *J. Phys. Chem. B* **2000**, *104*, 10174.

(13) El-ghayoury, A.; Schenning, A. P. J. H.; van Hal, P. A.; Van Duren, J. K. J.; Janssen, R. A. J.; Meijer, E. W. *Angew. Chem., Int. Ed.* **2001**, *40*, 3660.

(14) Marcos Ramos, A.; Rispens, M. T.; Van Duren, J. K. J.; Hummelen, J. C.; Janssen, R. A. J. *J. Am. Chem. Soc.* **2001**, *123*, 6714.

(15) De Boer, B.; Stalmach, U.; Van Hutten, P. F.; Melzer, C.; Krasnikov, V. V.; Hadziioannou, G. *Polymer* **2001**, *42*, 9097.

(16) (a) Wöhrle, D.; Meissner, D. *Adv. Mater.* **1991**, *3*, 129. (b) Schlettwein, D.; Wöhrle, D.; Karmann, E.; Melville, U. *Chem. Mater.* **1994**, *6*, 3. (c) Ferrere, S.; Zaban, A.; Gregg, B. A. *J. Phys. Chem. B* **1997**, *101*, 4490.

(17) Schmidt-Mende, L.; Fechtenkötter, A.; Müllen, K.; Moons, E.; Friend, R. H.; MacKenzie, J. D. *Science* **2001**, *293*, 1119.

(18) Dittmer, J. J.; Marseglia, E. A.; Friend, R. H. *Adv. Mater.* **2000**, *12*, 1270.

(19) Dittmer, J. J.; Petritsch, K.; Marseglia, E. A.; Friend, R. H.; Rost, H.; Holmes, A. B. *Synth. Met.* **1999**, *102*, 879.

(20) Angadi, M. A.; Gosztola, D.; Wasielewski, M. R. *J. Appl. Phys.***1998**, *83*, 6187.

(21) Miura, A.; Chen, Z.; Uji-i, H.; De Feyter, S.; Zdanowska, M.; Jonkheijm, P.; Schenning, A. P. H. J.; Meijer, E. W.; Würthner, F.; De Schryver, F. C. *J. Am. Chem. Soc.* **2003**, *125*, 14968.

(22) Marcos Ramos, A.; Knol, J.; Meskers, S. C. J.; van Hal, P. A.; Hummelen, J. C.; Janssen, R. A. J. *J. Phys. Chem. A* **2003**, *107*, 9269.

(23) Neuteboom, E. E.; van Hal, P. A.; Janssen, R. A. J. *Chem. Eur. J.* **2004**, *10*, 3907

(24) Weller, A. *Z. Phys. Chem. Neue Folge* **1982**, *133*, 93.

(25) Van Hal, P. A.; Beckers, E. H. A.; Peeters, E.; Apperloo, J. J.; Janssen, R. A. J. *Chem. Phys. Lett.* **2000**, *328*, 403.

(26) The assumption that charges are located at the centers of the chromophores is of course a simplification of the actual situation, in which charges are likely to be strongly delocalized.

(27) The molar absorption coefficients of the OPV chromophore at 700 and 900 nm have been extracted from the photoinduced absorption spectrum of a OPV/MP−C_{60} (1: 1) mixture in *o*-dichlorobenzene reported in ref 25, using the extinction coefficients of the MP−C_{60} reported in Guldi, D. M.; Prato, M. *Acc. Chem. Res.* **2000**, *33*, 695−703.

(28) Salbeck, J. *J. Electroanal. Chem.* **1992**, *340*, 169.

(29) In this situation the energy transfer has to be subpicosecond. Förster theory allows estimation of the energy transfer rate by using the overlap of the OPV emission and PERY absorption, the lifetime of the OPV singlet state, and the OPV fluorescence quantum yield. This provides a Förster

radius of about 55 Å and an energy transfer faster than 500 fs at distances less than 15 Å for the distance between the two chromophores. This distance is somewhat shorter than the actual distance of 21 Å.

(30) (a) Marcus, R. A. *J. Chem. Phys.* **1965**, *43*, 679−701. (b) Marcus, R. A. *Angew. Chem., Int. Ed. Engl.* **1993**, *32*, 1111.

(31) Oevering, H.; Paddon-Row, M. N.; Heppener, M.; Oliver, A. M.; Cotsaris, E.; Verhoeven, J. W.; Hush, N. S. *J. Am. Chem. Soc.* **1987**, *109*, 3258.

(32) Kroon, J.; Oevering, H.; Verhoeven, J. W.; Warman, J. M.; Oliver, A. M.; Paddon-Row, M. N. *J. Phys. Chem.* **1993**, *97*, 5065.